Quasimonoenergetic Proton Bunch Generation by Dual-Peaked Electrostatic-Field Acceleration in Foils Irradiated by an Intense Linearly Polarized Laser

H. B. Zhuo (卓红斌),[1,2] Z. L. Chen (陈正林),[1,*] W. Yu (余玮),[3] Z. M. Sheng (盛政明),[4,5] M. Y. Yu (郁明阳),[6,7] Z. Jin (金展),[1] and R. Kodama (兒玉了祐)[1,8]

[1]*Graduate School of Engineering, Osaka University, 2-1 Yamada-oka, Suita, Osaka 565-0871, Japan*
[2]*National Laboratory for Parallel and Distributed Processing, School of Computer Science, National University of Defense Technology, Changsha 410073, People's Republic of China*
[3]*Shanghai Institute of Optics and Fine Mechanics, Chinese Academy of Sciences, Shanghai 201800, People's Republic of China*
[4]*Department of Physics, Shanghai Jiao Tong University, Shanghai 200240, People's Republic of China*
[5]*Beijing National Laboratory for Condensed Matter Physics, Institute of Physics, CAS, Beijing 100080, People's Republic of China*
[6]*Institute for Fusion Theory and Simulation, Zhejiang University, Hangzhou 310027, People's Republic of China*
[7]*Institute for Theoretical Physics I, Ruhr University, Bochum D-44780, Germany*
[8]*Institute of Laser Engineering, Osaka University, 2-6 Yamada-oka, Suita Osaka 565-0871, Japan*

(Received 5 November 2009; published 5 August 2010)

It is found that stable proton acceleration from a thin foil irradiated by a linearly polarized ultraintense laser can be realized for appropriate foil thickness and laser intensity. A dual-peaked electrostatic field, originating from the oscillating and nonoscillating components of the laser ponderomotive force, is formed around the foil surfaces. This field combines radiation-pressure acceleration and target normal sheath acceleration to produce a single quasimonoenergetic ion bunch. A criterion for this mechanism to be operative is obtained and verified by two-dimensional particle-in-cell simulation. At a laser intensity of $\sim 5.5 \times 10^{22}$ W/cm^2, quasimonoenergetic GeV proton bunches are obtained with $\sim$100 MeV energy spread, less than 4° spatial divergence, and $\sim$50% energy conversion efficiency from the laser.

DOI: 10.1103/PhysRevLett.105.065003 PACS numbers: 52.38.Kd, 29.25.−t, 52.50.Jm, 52.65.Rr

High-quality energetic ion bunches have many potential applications [1], including medical isotope generation, proton imaging and oncology, injector for traditional ion accelerators, nuclear physics, high energy physics, fast ignition in inertial confined fusion, and diagnostics of future tokamaks. Several mechanisms for ion acceleration from the interaction of a laser with thin solid targets have been studied theoretically and experimentally [2–8]. Three main acceleration regimes have been identified: target normal sheath acceleration (TNSA) [3], radiation-pressure acceleration (RPA) [4], and breakout afterburner acceleration (BOA) [5]. In TNSA, ions are accelerated by the target-backside sheath potential produced by the laser-ejected target electrons. The energetic ions in this regime usually have continuous energy spectra and a cutoff energy, which barely reach $\sim$100 MeV/nucleon [6]. In RPA, the radiation pressure at the front surface accelerates and compresses the target electrons, creating an intense space-charge field that accelerates the ions. In this regime monoenergetic GeV proton beams can be produced, although certain extreme conditions for the laser beam, such as extremely high laser intensity, sharp rising front, and ultrathin target thickness, are mandatory [7]. Also it is favorable to avoid generating hot electrons with circularly polarized laser pulses [8]. The BOA mechanism, on the other hand, appears as a consequence of dynamics associated with the nonlinear transparency of the laser pulse and enhanced electron heating, combing with the beam-plasma instability [5]. The BOA can dramatically improve the acceleration efficiency as compared with the TNSA and require a significantly lower laser intensity than for RPA.

In this Letter, we present another mechanism, namely, the dual-peaked electrostatic-field acceleration (DEFA), for accelerating the protons in a thin foil target by using a linearly polarized ultraintense laser. DEFA makes use of RPA and TNSA, respectively, at the front and back sides of the foil. Together they form a self-consistent dual-peaked electrostatic space-charge field. Under appropriate conditions, this field can persistently trap target protons and accelerate them monoenergetically to the GeV level. The resulting proton bunch also has narrow energy spread, small spatial divergence, and high laser-energy conversion efficiency.

A one-dimensional model of the DEFA configuration is depicted in Fig. 1. The two electric field peaks are due to the two components of the ponderomotive force of the linearly polarized laser [9]: the nonoscillating part $-(e^2/4m_e\omega_0^2)\nabla E^2(x)$ and the oscillating part $-(e^2/4m_e\omega_0^2)\cos(2\omega_0 t)\nabla E^2(x)$, where $E(x)$ is laser electric field amplitude, m_e is electron mass, e is electron charge, and ω_0 is laser frequency. The nonoscillating component accelerates the electrons at the target front surface (region I) deep into the foil (region II), forming the electrostatic field E_{front}, which accelerates the protons in region I. The peak of this electrostatic field can be estimated to be $4I_0/en_0cD$, where I_0 is the laser intensity,

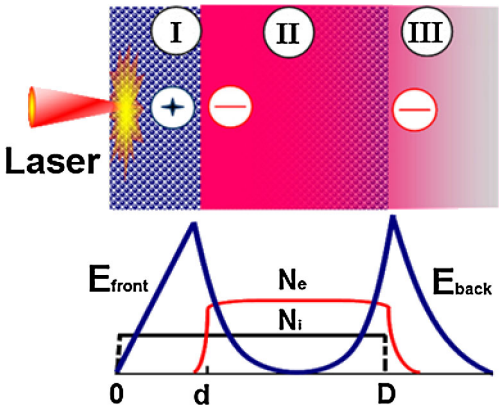

FIG. 1 (color online). Schematics of the dual-peaked electrostatic-field acceleration of protons. There are three regions: depleted electron region with thickness d (region I), dumped electron region (region II), and escaped electron region (region III). The first two are within the foil, and region III is in the target-back vacuum. Blue and red represent the protons and electrons, respectively. The profiles of the electric fields and density distributions of the electrons and protons are sketched in the lower panel.

n_0 is the initial electron density, D is the foil thickness, and c is the light speed, by balancing the radiation and charge-separation forces [4]. The oscillating component of the ponderomotive force rapidly accelerates and heats the foil electrons. Many of these electrons pass through the foil to the rear vacuum (region III), generating a space-charge field $E_{\text{back}} \approx (4\pi n_0 K_B T_e)^{1/2}$ [10]. The hot-electron temperature T_e in region II is given by [11] $T = T_{e,\text{Wilks}} = [(1 + a_0^2)^{1/2} - 1]m_e c^2$, where a_0 is the normalized laser amplitude. The electrostatic field E_{back} then accelerates the protons in region II. In order for the protons to be steadily accelerated to the GeV level, an appropriate foil thickness for realizing a rough balance of E_{front} and E_{back} is needed. Balance between the radiation-pressure and the space-charge forces in region I gives $a_0/\sqrt{2}\pi n_0 \leq D$ (similar to that for circularly polarized lasers [8]), where n_0 and D have been normalized by the critical density n_c and laser wavelength λ_0, respectively. On the other hand, stable proton acceleration requires $E_{\text{front}} \geq E_{\text{back}}$ in order for all the accelerating foil protons to remain trapped throughout the acceleration process. Combining these requirements, we obtain the condition

$$(\sqrt{2}\pi)^{-1} a_0/n_0 < D < \pi^{-1}(a_0/n_0)^{3/2} \qquad (1)$$

for stable proton acceleration, and $a_0 > n_0/2$ is mandatory. The corresponding proton momentum obtained from Ref. [7] is

$$\frac{d}{dt}u_i = \frac{a_0^2}{n_0 M D}\frac{\sqrt{1+u_i^2}-u_i}{\sqrt{1+u_i^2}+u_i}, \qquad (2)$$

where $u_i = P_i/m_i c$ is the normalized momentum, t is the time normalized by the laser period τ_0, $M = m_i/m_e$, and m_i is proton static mass. Equation (2) provides an estimate for the maximum proton energy [7]: $\varepsilon_{i\,\max} = 2\eta^2\varepsilon_L^2/(2\eta\varepsilon_L + N_i m_i c^2)N_i$, where η is the efficiency of energy transfer from the laser to the protons, ε_L is the laser pulse energy, and N_i is the proton number.

To verify the DEFA mechanism, we carry out two-dimensional (2D) particle-in-cell (PIC) simulations using the code PDLPICC2D [12]. The simulation box is $50\lambda_0 \times 40\lambda_0$ with a spatial resolution up to 200 cells per wavelength. Each cell contains 36 ions and 36 electrons. The fully ionized proton plasma foil of initial density $n = 100n_c$ is $0.8\lambda_0$ thick and $40\lambda_0$ wide, with its front surface located at $x = 4\lambda_0$. The initial electron temperature is 5 keV, and the ions are cold. The linearly polarized trapezoidal laser pulse with the super-Gaussian intensity distribution $\exp[-(r/r_0)^4]$ propagates along the x direction, where $r_0 = 10\lambda_0$ is the spot radius. It has a duration $10\tau_0$, consisting of a plateau region of $8\tau_0$ and rising and falling times of $1\tau_0$ each. Its amplitude is $a_0 = 200$, corresponding to the laser intensity $I = 5.5 \times 10^{22}$ W/cm^2. An absorbing boundary condition is adopted for both the electromagnetic waves and simulation particles. An exact charge conservation scheme [13] and simulation particles with a fourth-order form factor are used in our simulation to suppress numerical noise.

Figure 2 shows the simulation results for three foil thicknesses: one ($D = 0.8\lambda_0$) satisfying (1) and other two ($D = 0.3\lambda_0$ and $5.0\lambda_0$) not. As shown in Fig. 2(a), although the maximum proton energy in all the three cases is larger than 1 GeV, a quasimonoenergetic proton beam at

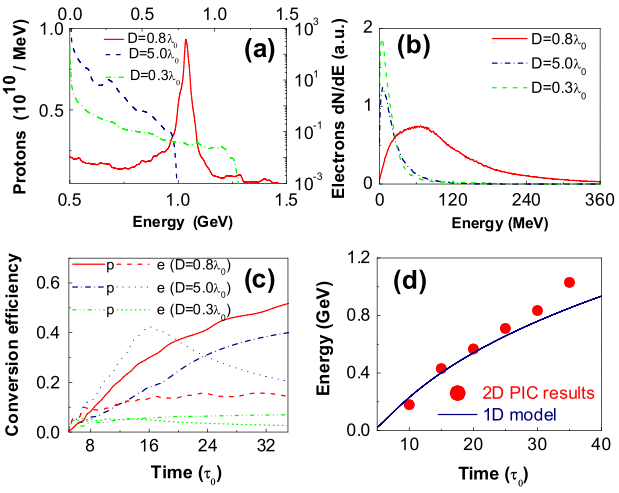

FIG. 2 (color online). (a) Proton energy spectra at $t = 35\tau_0$ for $D = 0.8\lambda_0$, $5.0\lambda_0$, and $0.3\lambda_0$, with the top and right axes for the non-DEFA cases $D = 5.0\lambda_0$ and $0.3\lambda_0$. (b) The electron energy spectra collected at the surface $x = 50\lambda_0$ for the three cases. (c) Evolution of the efficiencies of energy conversion to protons (p) and electrons (e) for the three cases. (d) Peak energies of proton beams versus time for $D = 0.8\lambda_0$.

~1 GeV is observed only when the foil thickness satisfies (1). The full-width-at-half-maximum energy spread is as narrow as ~100 MeV. We see in Fig. 2(b) for $D = 0.8\lambda_0$ that there is a large number of hot electrons, peaked at ~60 MeV, such that the proton acceleration is nearly quasineutral. If the foil is either too thick or too thin according to Eq. (2), the electron energy distribution exhibits the normal thermal spectra with high energy tails, as usually found for linearly polarized lasers [3]. Figure 2(c) shows that for $D = 0.8\lambda_0$, the energy conversion efficiency from the laser to the protons is as large as 50%, also much larger than that in the other two cases. The efficiency of energy conversion from the laser to the hot electrons is also shown. The thicker the foil is, the more the laser energy is transferred to the electrons (rather than to the protons). When the foil is thinner than the lower limit of (1), the efficiencies of energy conversion from the laser to the electrons and protons are both low. This is because of the premature breaking of the foil plasma and the resulting free passage of the laser pulse without further interaction with the plasma. Figure 2(d) shows the peak energy of the proton bunch as a function of time for $D = 0.8\lambda_0$, which is in good agreement with that obtained from the analytical model [Eq. (2)].

The acceleration process can be better understood by inspecting the induced-field structures. Figure 3(a) shows that near the foil front and back surfaces the electrostatic field has two peaks, at $x = 17.2\lambda_0$ and $x = 17.8\lambda_0$, respectively. These are the space-charge fields created by the electrons expelled by the nonoscillating ponderomotive force and from the energetic hot electrons expelled by the oscillating ponderomotive force, respectively, as invoked in the one-dimensional analytical model above. The proton and net charge distributions in Fig. 3(a) have similar two-peak structures, indicating the presence of concurrent acceleration in both regions. The evolution of the dual-peaked electrostatic field is shown in Fig. 3(b). It has a quasiperiodic structure, indicating that the balance between the ponderomotive and the electric forces is dynamic: The front peak is first built up, before proton acceleration at the front takes place. As the fast laser-driven front electrons are expelled to the target rear side, a sheath field is built up behind the target. It accelerates the target-backside protons as well as the protons arriving there after being preaccelerated in the front part of the target. In the entire acceleration process the target remains opaque to the laser and the two-peaked structure is stably maintained, leading to stable DEFA acceleration. The simulated field evolution also agrees well with that predicted by Eq. (2) of the analytical model.

Figure 4 shows the two proton bunches accelerated by the two electric field peaks in Fig. 3. The trajectories of the electrons indicate that most electrons move together with the protons, and only a small number of hot electrons escape from the foil. The periodic structure is associated with the efficient and stable energy transfer from the laser to the protons and the electron energy spectrum in Fig. 2(b).

The proton spatial and momentum distributions in Fig. 5 show in more detail the DEFA process. At $t = 10\tau_0$, a locally delimited plasma disk corresponding exactly to the laser spot is accelerated forward by the laser. The protons in the foil back surface are accelerated more strongly than that in the front surface, indicating rapid electron heating and expansion into the backside vacuum. At $t = 20\tau_0$, the acceleration is steady, and the pouchlike low-density plasma structure behind the accelerating protons traps the laser pulse. Figure 5(c) shows that at $t = 35\tau_0$, or the end of the acceleration process, the pouchlike wake structure is disappearing and the accelerated monoenergetic proton layer has arrived at $x = 23\lambda_0$ (from the original $x = 4\lambda_0$) with a peak energy of 1.0 GeV, peak density $>50n_c$, and spatial divergence $<4°$ [calculated from the data for Fig. 5(e)]. Figure 5(d) shows that the protons have good monoenergetic and collimation characteristics. A feature similar to wave breaking can be seen in Fig. 5(e), which shows that the protons from the front acceleration region can catch up with that from the target-back acceleration

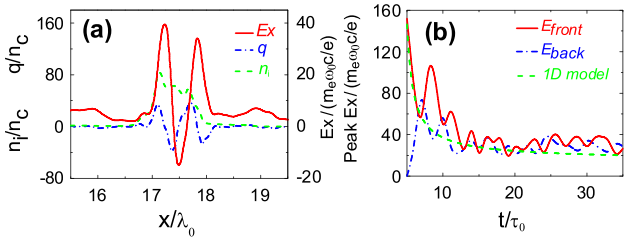

FIG. 3 (color online). (a) Ion density n_i/n_c, charge density q/n_c, and the longitudinal electric field E_x on the laser axis at $t = 25\tau_0$. (b) Evolution of the two peaks of E_x at the foil front and back sides. The green dashed line is from the analytical model.

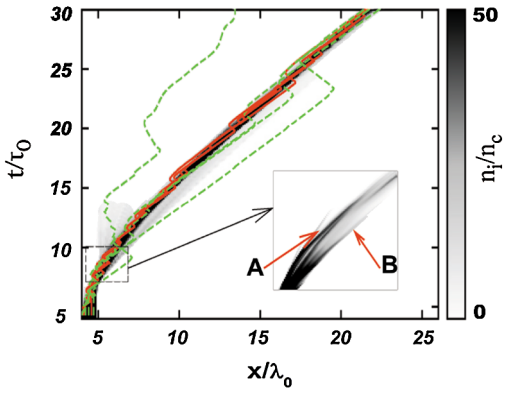

FIG. 4 (color online). The proton density n_i/n_c (gray) along the laser axis and typical electron trajectories (green and red dashed lines). The inset gives an enlarged view of the fine structure inside the dashed rectangle, showing the two proton beams A and B.

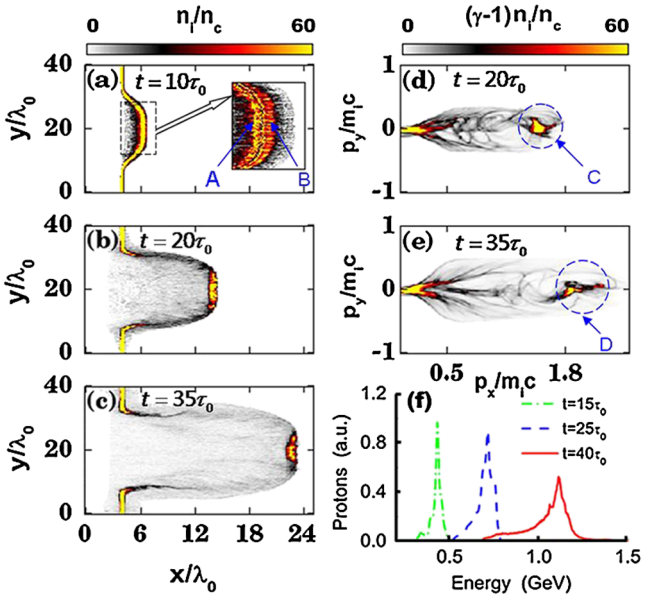

FIG. 5 (color online). The proton density at (a) $t = 10\tau_0$, (b) $t = 20\tau_0$, and (c) $t = 35\tau_0$, the proton momentum at (d) $t = 20\tau_0$ and (e) $t = 35\tau_0$, and (f) the evolution of the proton energy spectrum. A and B in (a) mark the two accelerating proton bunches. Shown in (d) is the proton beam (marked C) in the stable acceleration stage, and shown in (f) is the disintegrating proton bunch (marked D) at the end of the acceleration.

region. However, at a still later stage the energy and spatial spreads both increase because of expansion of the bunch. Figure 5(f) for the evolution of the proton spectrum shows the stable acceleration of the quasimonoenergetic proton bunches during the acceleration stage.

Stable DEFA ends when the target becomes transparent due to expansion. After the laser has penetrated through the target, the electrons are scattered away by the laser field and the dual-peaked electrostatic field disappears. At the same time, the proton bunch collapses and its energy spread increases quickly. Therefore, proper length of the laser pulse is critical for generating a high-quality monoenergetic proton beam. In this simulation the laser pulse is about 33 fs; the laser is terminated before transmitting through the target.

Although the simulation results described so far are for the special pulse profile, such an extreme condition is actually not necessary for the DEFA mechanism as long as (1) is satisfied. For example, with the practically Gaussian shape of the laser, $I \sim I_0 \exp[-(r/r_0)^2]\exp\{-[(t-3t_0)^2/t_0^2]\}$, where $r_0 = 10\lambda_0$ and $t_0 = 5\tau_0$ are taken and the other parameters are the same as in Fig. 5, our simulations verify that typical DEFA behavior can also clearly be observed. A quasimonoenergetic proton bunch around ~700 MeV with ~100 MeV energy spread and less than 10° spatial divergence is obtained in 2D simulation results.

In conclusion, we have investigated a new regime, namely, DEFA, for achieving high-quality well collimated quasimonoenergetic GeV proton beams. The DEFA regime makes use of the two space-charge fields formed near the front and back surfaces of the thin foil formed by the nonoscillating and oscillating components of the laser ponderomotive force, respectively. Two-dimensional PIC simulations demonstrate the production of high-quality proton beams under the criterion for DEFA. With this mechanism, it appears possible to achieve multi-100 MeV proton beams for medical therapy with lasers presently available at focused intensity 5×10^{21} W/cm^2 in 50 fs.

We thank H. B. Cai for useful discussions. This work is supported by the Core Research for Evolutional Science and Technology of Japan Science and Technology Agency and by the National Natural Science Foundation of China (Grants No. 10505030, No. 10734130, No. 10835003, No. 10975185, No. 60970033, and No. 10935002), the National High-Tech ICF Committee of China, the National Basic Research Program of China (Grants No. 2007CB815105, No. 2008CB717806, No. 2009GB105002, and No. 2009GB105005), and the National High Technology Research and Development Program of China (Grant No. 2008AA012317).

*To whom correspondence should be addressed.
zhenglinchen.czl@gmail.com

[1] L. Robson *et al.*, Nature Phys. **3**, 58 (2007), and references therein.
[2] M. Zepf *et al.*, Phys. Rev. Lett. **90**, 064801 (2003); M. S. Wei *et al.*, Phys. Rev. Lett. **93**, 155003 (2004); H. Habara *et al.*, Phys. Rev. E **69**, 036407 (2004); B. M. Hegelich *et al.*, Nature (London) **439**, 441 (2006); H. Schwoerer *et al.*, Nature (London) **439**, 445 (2006).
[3] S. C. Wilks *et al.*, Phys. Plasmas **8**, 542 (2001); A. Pukhov, Phys. Rev. Lett. **86**, 3562 (2001).
[4] A. Macchi *et al.*, Phys. Rev. Lett. **94**, 165003 (2005); A. P. Robinson *et al.*, New J. Phys. **10**, 013021 (2008); X. Q. Yan *et al.*, Phys. Rev. Lett. **100**, 135003 (2008); T. V. Liseykina *et al.*, Plasma Phys. Controlled Fusion **50**, 124033 (2008).
[5] L. Yin *et al.*, Laser Part. Beams **24**, 291 (2006); L. Yin, Phys. Plasmas **14**, 056706 (2007).
[6] S. P. Hatchett *et al.*, Phys. Plasmas **7**, 2076 (2000).
[7] T. Esirkepov *et al.*, Phys. Rev. Lett. **92**, 175003 (2004).
[8] X. Q. Yan *et al.*, Phys. Rev. Lett. **103**, 135001 (2009); M. Chen *et al.*, Phys. Rev. Lett. **103**, 024801 (2009).
[9] W. L. Kruer, *The Physics of Laser Plasma Interactions* (Addison-Wesley, New York, 1998).
[10] V. Yu. Bychenkov *et al.*, Phys. Plasmas **11**, 3242 (2004).
[11] S. C. Wilks *et al.*, Phys. Rev. Lett. **69**, 1383 (1992).
[12] H. B. Zhuo *et al.*, Phys. Rev. E **79**, 015401 (2009).
[13] T. Zh. Esirkepov *et al.*, Comput. Phys. Commun. **135**, 144 (2001).